ISSN 1054-660X, Laser Physics, 2008, Vol. 18, No. 2, pp. 165–174.

Short Optical Pulse Profile Characterization Using a Nonlinear Optical Loop Mirror

O. Pottiez[a], *, B. Ibarra-Escamilla[b], **, and E. A. Kuzin[b], ***

[a] *Centro de Investigaciones en Óptica (CIO), Loma del Bosque 115, Col. Lomas del Campestre, León, Gto 37150, Mexico*
[b] *Instituto National de Astrofisica, Óptica y Electrónica (INAOE), L. E. Erro 1, Tonantzintla, Puebla, Pue 72000, Mexico*

*e-mail: pottiez@cio.mx
**e-mail: baldemar@inaoep.mx
***e-mail: ekuz@inaoep.mx

Received August 23, 2007

Abstract—We propose in this work a technique for short pulse profile retrieval based on the Kerr effect in a fiber nonlinear optical loop mirror (NOLM). Under some assumptions, the profile can be determined from the energy transfer characteristic of the pulses through the NOLM, which can be measured with a low-frequency detection setup. Two numerical approaches are considered, both relying on the resolution of a system of nonlinear algebraic equations, and which differ in the way that the profiles are discretized. We show numerically that both approaches allow proper profile retrieval for a wide variety of pulse shapes. The two techniques are compared, and their advantages and drawbacks are discussed. The effect of the amplitude noise of the pulses is assessed, as well as the impact of an inaccurate knowledge of the NOLM transfer function, or of the energy transfer characteristic. The technique is demonstrated in the frame of the characterization of both *ns* and *ps* pulses.

PACS numbers: 42.81.-i; 42.30.Lr

DOI: 10.1134/S1054660X08020114

1. INTRODUCTION

In order to improve our understanding of the physics of pulsed lasers, and for a growing number of applications making use of these sources, knowledge of the temporal profile of the pulses is essential. Convenient measurement of pulse features whose duration is below the response time of the fastest optoelectronic devices remains, however, a challenge. Several techniques use an ultrafast nonlinear optical process to achieve this task [1–9]. The widespread optical autocorrelation technique [1, 2] can be used to infer pulse duration, if a particular pulse profile can be assumed. Allowing measurement of pulse durations down to the *fs* range, this technique can also be readily extended to achieve complete pulse profile retrieval (amplitude and phase) [3–6]. However, the free-space implementation of the device and the phase-matching requirement (if the nonlinear process is the second-harmonic generation) impose careful beam alignment and crystal orientation and cause enhanced sensitivity to perturbations (note that phase matching is not required if two-photon absorption [6] is used as the nonlinear process). Moreover, the mechanically imposed scanning range limits the flexibility of the measurement span. Linear techniques were also developed for the complete characterization of ultrashort pulses, being usually simpler in processing and requiring much lower intensities than nonlinear techniques [10–14]. The drawbacks, however, include the need for complex electronics [10] or high-speed detection [11–14]. Note, finally, that some "linear" techniques developed for measuring ultraweak pulses rely, in fact, on the use of a nonlinear method to precisely characterize a reference pulse [15, 16]. Alternatives can be figured out if the shape only of somewhat longer (>1 ps) pulses is to be determined. On the other hand, although >20 ps pulses can be readily measured using a 50-GHz photodetector and sampling scope, high-speed detection is expensive, so that there is interest in developing simple and affordable techniques to characterize pulses in the *ps* to *ns* range.

The fiber nonlinear optical loop mirror (NOLM) [17] is a versatile device that has been used for ultrafast switching, signal processing, or optical data monitoring [18]. Here, we propose a NOLM-based technique to retrieve the profile of short optical pulses. The Kerr effect in silica fiber is used, which requires no phase matching. An all-fiber solution avoids alignment issues, ensures a high robustness, and reduces costs [14], whereas the Sagnac architecture (in which both beams travel along the same path) improves the stability.

The power transfer characteristic of a NOLM $T = P_{out}/P_{in}$ (where P_{in} and P_{out} are input and output powers, respectively) is a sinusoidal function of P_{in} [17]. Assuming a zero minimal transmission, T becomes

$$T = K\left[\frac{1}{2} - \frac{1}{2}\cos(\pi P_{in}/P_{\pi} - \Delta\phi)\right], \qquad (1)$$

where P_{π} is the critical power, K is the maximum transmission, and $\Delta\phi$ is the phase bias. The transmission curves for three different values of $\Delta\phi$ are presented in Fig. 1a. If $\Delta\phi > 0$, $T = 0$ at power $p_z = \Delta\phi P_{\pi}/\pi$. Now, if

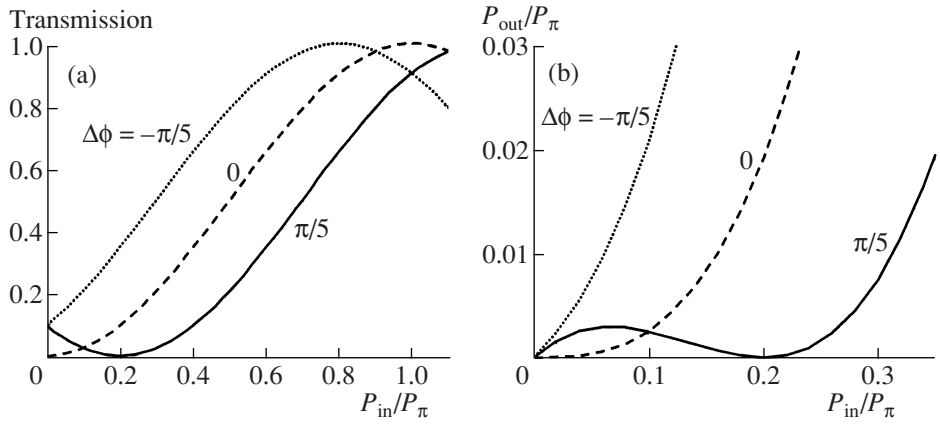

Fig. 1. (a) Transmission and (b) output power characteristics of an NOLM with a zero minimal transmission for different values of $\Delta\phi$.

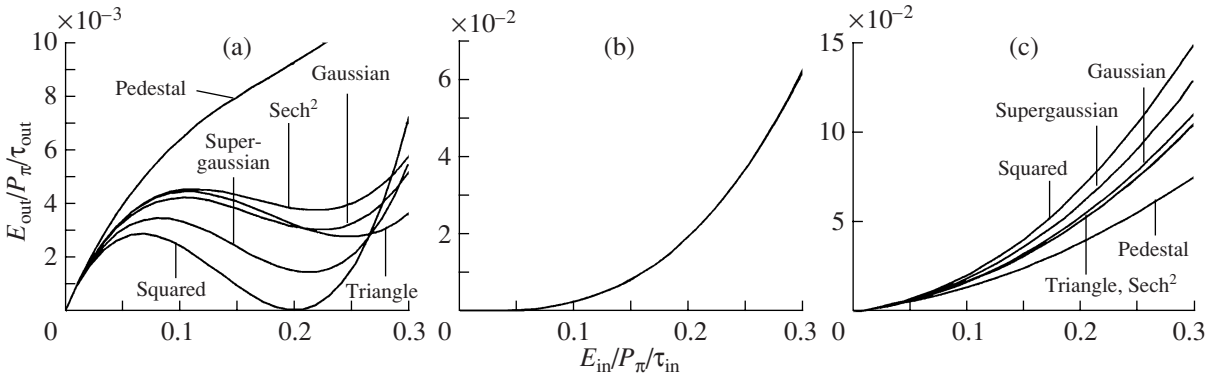

Fig. 2. Normalized output pulse energy versus input pulse energy for several pulse profiles defined by the curve labels (see Fig. 4), where $\Delta\phi = \pi/5$ (a), 0 (b), and $-\pi/5$ (c). $Sech^2$, squared hyperbolic secant; Supergaussian, squared Gaussian.

a pulse with power profile $p(t)$ is launched at the NOLM input, the output profile is $P_{out}[p(t)]$, where $P_{out}(P_{in}) = T(P_{in})P_{in}$ is the output power characteristic of the NOLM (Fig. 1b). The output pulse energy E_{out} is obtained by integrating $P_{out}[p(t)]$ over time:

$$E_{out} = \int P_{out}[p(t)]dt.$$

Figure 2 shows E_{out} versus input pulse energy E_{in} for different pulse profiles for the three values of the phase bias $\Delta\phi$ considered in Fig. 1. Energies are normalized with respect to pulse duration τ_{in} or τ_{out} at the NOLM input or output, respectively, defined as

$$\tau_{in} = \int_{-\infty}^{\infty} p(t)/p_{max}dt;$$
$$\tau_{out} = \lim_{p_{max}\to 0}\left[\int_{-\infty}^{\infty} P_{out}[p(t)]/P_{out}(p_{max})dt\right], \quad (2)$$

where p_{max} is the peak pulse power. With these definitions, $\tau_{in/out}$ is the duration of the equivalent squared pulse having the same energy and peak power as the actual pulse. In the case of τ_{out}, the limit indicates that the NOLM transmission at a low power is considered. If $T(0) \neq 0$ ($\Delta\phi \neq 0$), $P_{out}(p) \approx T(0)p$ at a low power and $\tau_{out} = \tau_{in}$. Now, if $T(0) = 0$ ($\Delta\phi = 0$), $T(p) \propto p^2$, $P_{out}(p) \propto p^3$ at a low power and $\tau_{out} = \int p^3(t)/p_{max}^3 dt$.

Let us first consider Fig. 2a, obtained for a positive value of $\Delta\phi$. It clearly appears that each profile has a specific E_{out} characteristic. This can be understood by considering that each pulse profile "stays" for a specific time around each particular value of power (between 0 and the peak power). For example, the "squared" profile stays at the same power level over the entire pulse duration, so that the E_{out} characteristic reproduces the P_{out} characteristic of the NOLM, in particular, decaying to zero for peak power p_z. In contrast, all other pulse profiles present skirts at powers lower than the peak.

Hence, even when the peak power reaches p_z, the skirts yield nonzero values of P_{out}, which prevents E_{out} from getting back to zero for nonzero values of E_{in}. The E_{out} characteristic still presents a local minimum for these profiles, except in the "pedestal" case, since a large portion of the pulse energy is then well below the peak power. The specificity of the E_{out} characteristic for each pulse shape can be exploited to retrieve the pulse profile from pulse-energy measurements.

For other values of the bias, however, the E_{out} characteristic is not so specific to a particular pulse shape. If $\Delta\phi = 0$ (Fig. 2b), all of the characteristics are superimposed at a low power. In this case, $P_{out}(p) \propto p^3$ and $E_{out} \propto \tau_{out} p_{max}^3$ for all profiles. For $\Delta\phi < 0$ (Fig. 2c), the E_{out} curves appear to be distinct, but they are more closely packed than in Fig. 2a (over the same power range). This is due to the smaller dynamic range of T at a moderate power, which no longer decays to zero, but slowly grows with P_{in}. This yields a poor robustness for the profile discrimination, which will appear later.

2. VERTICAL SLICING

This technique was first demonstrated in [19]. We consider an NOLM whose T (or P_{out}) characteristic is perfectly known. The unknown profile is decomposed into a series of N rectangular slices of duration δt, much smaller than the pulse width, each having a power equal to the instantaneous pulse power at the center of the corresponding interval (Fig. 3). At the NOLM output, each rectangle of duration δt and power p yields a rectangle of the same duration and power $P_{out}(p)$. The output pulse energy is then identified to the energy of all the rectangles through the NOLM, yielding

$$\sum_{j=1}^{N} P_{out}(a_i p_j)\delta t = E_{out}(a_i), \quad i = 1, \ldots, M, \qquad (3)$$

where the a_i are attenuation (or amplification) coefficients of the input pulse power. Equation (3) is a system of nonlinear algebraic equations, whose unknown quantities are the instantaneous power values p_j, $j = 1, \ldots, N$, and the interval duration δt. A necessary condition for this system to be determined is that the number of equations M be at least equal to $N + 1$. This means that the estimation of the pulse profile at N points requires the measurement of E_{out} for at least $M = N + 1$ different values of a_i. To avoid multiple solutions, more than $N + 1$ values of a_i can be considered ($M > N + 1$, overdetermined system). Equation (3) can be solved numerically for p_j and δt. Alternatively, one can observe from Eq. (3) that, using one of the equations, say the Mth one, δt can be expressed in terms of the other variables, and then substituted into the $M - 1$ remaining equations. The system is then rewritten as

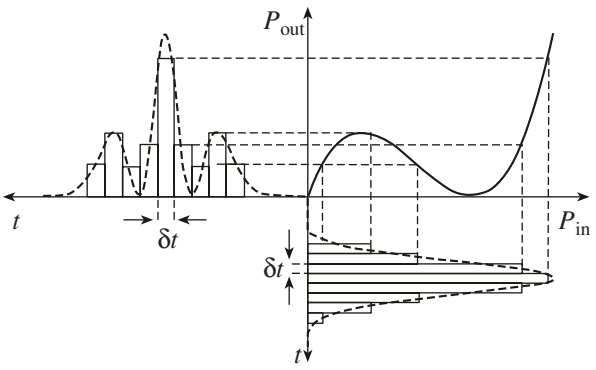

Fig. 3. Principle of vertical slicing operation.

$$\frac{\sum_{j=1}^{N} P_{out}(a_i p_j)}{\sum_{j=1}^{N} P_{out}(a_M p_j)} = \frac{E_{out}(a_i)}{E_{out}(a_M)} \quad i = 1, \ldots, M-1. \qquad (4)$$

This system must be solved numerically for the N variables p_j. The main advantage of solving Eq. (4) instead of Eq. (3) is that no initial estimate of δt (thus, of pulse duration) is required. Once the p_j are known, δt can be calculated directly using $\delta t = E_{out}(a_i)/\sum P_{out}(a_i p_j)$ for any value of i.

Even if there is only one set of values p_j yielding a particular E_{out} characteristic, the order of the succession of slices across the profile cannot be determined. Indeed, the measured pulse energy contains no information about the relative timing of the rectangles. To raise the indetermination, some assumption is required. Here, we assume that the profile decreases monotonically from its peak (thus, discarding possible troughs in the pulse shape), either on one side (single-sided profile) or symmetrically on both sides (symmetric profile).

This method was tested numerically for different symmetric pulse profiles (Fig. 4). Transmission T was given by Eq. (1) with $\Delta\phi = \pi/5$, yielding zero at a moderate power $p_z = 0.2P_\pi$. The E_{out} characteristic was simulated for each profile through numerical integration of $P_{out}[a_i p(t)]$. Peak powers ranged from $a_i = 0$ to ~$0.3P_\pi$, thus using T far below a critical power. In each case, we solved Eq. (4) numerically using the least-squares method. A symmetric profile was assumed. A Gaussian profile was chosen for the initial estimations of p_j (the results did not depend critically on this choice). We used $N \approx 20$ points across the half profile, and $M - N \approx$ 1–5. Proper convergence and profile recovery were observed for an initial peak power guess in the range of –10 dB about its actual value. An issue, however, is that

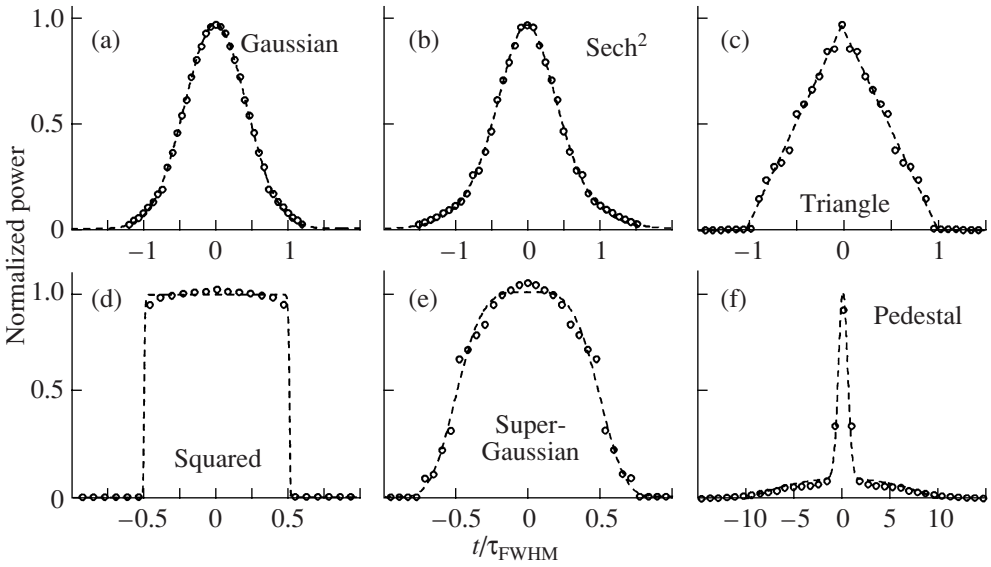

Fig. 4. Results of the vertical slicing technique for several pulse profiles: (a) Gaussian; (b) squared hyperbolic secant (soliton); (c) triangular; (d) rectangular; (e) supergaussian (or squared Gaussian); and (f) Gaussian with pedestal. Circles and dashed line show the optimized powers and target profiles, respectively, and τ_{FWHM} is the pulse duration.

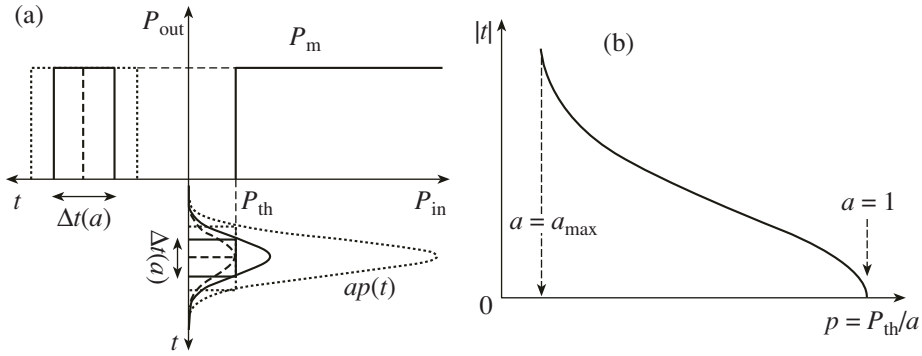

Fig. 5. (a) Principle of horizontal slicing operation in the ideal case of a step-power transfer function; (b) recovered pulse profile.

sharp edges are only outlined by a few points (see Figs. 4d–4f).

Although the choice of $\Delta\phi$ is not critical, it should be $\neq 0$, since convergence is not observed in this case. Indeed, if $\Delta\phi = 0$, the E_{out} characteristic is not specific to a particular pulse shape, as mentioned earlier (Fig. 2b), and indetermination arises in Eq. (4). In contrast, if $\Delta\phi < 0$, profile recovery is still observed.

3. HORIZONTAL SLICING

An alternative approach can be figured out, as described in the following. We, first, consider an ideal step-like output power characteristic, equal to zero for input power levels P_{in} below a threshold value P_{th}, and to a nonzero constant value P_m above this threshold (Fig. 5a). We, again, assume that the input pulse power can be adjusted (amplified or attenuated) by a known coefficient a before entering the NOLM, so that the input pulse profile becomes $ap(t)$. Let us assume that $a = 1$ when the peak power reaches P_{th}. If the input peak power is above P_{th} ($a > 1$), the output pulse has a rectangular profile, with a maximum value P_m and a duration Δt equal to the temporal width of the input pulse taken at the power $ap(t) = P_{th}$, i.e., at $p = P_{th}/a$. Note that the same output waveform would be obtained considering at the input a rectangular pulse with duration Δt and a power equal or superior to P_{th} (Fig. 5a). The output average power is thus given by $E_{out}(a) = P_m\Delta t(a)$. The measurement of $E_{out}(a)$ for various values of a thus directly yields $\Delta t(a) = E_{out}(a)/P_m$, which can be plotted as a function of $p = P_{th}/a$ (Fig. 5b). Assuming that the

pulse decays monotonically from its peak, symmetrically on both sides (or asymmetrically on one side), this procedure determines the pulse profile $p(t)$, with $|t| = \Delta t/2$ ($|t| = \Delta t$, respectively) for instantaneous power values higher than $p = P_{th}/a_{max}$, where a_{max} is the maximum value of a.

To extend the idea to a real, nonstep-like power characteristic, like that of an NOLM, we divide the P_{in} axis into a finite number of small power intervals $a\Delta p$ (where a is an adjustment factor) over which P_{out} is assumed to be constant, and equal to the output power at the center of the interval. The P_{out} characteristic is, thus, approximated by a staircase-like function (Fig. 6). With that characteristic, the output pulse profile is a superposition of rectangular blocks (see Fig. 6). Note that this output pulse profile is unchanged if the input pulse $p(t)$ is replaced by a stack of rectangles of height Δp and width $\Delta t_j = \Delta t(j\Delta p)$, $j = 0, \ldots, N-1$. The output pulse energy corresponds to the sum of the areas of all of the rectangles in the output profile. If E_{out} is measured for M values of input power, we have

$$\sum_{j=0}^{N-1} \Delta P_j(a_i\Delta p)\Delta t_j = E_{out}(a_i), \quad i = 1, \ldots, M, \quad (5)$$

where $\Delta P_j(a_i\Delta p)$ is the jump of the output power that occurs in the staircase transfer characteristic at $P_{in} = ja_i\Delta p$. It is given by

$$\Delta P_0(a_i\Delta p) = P_{out}\left[\frac{1}{2}a_i\Delta p\right];$$
$$\Delta P_j(a_i\Delta p) = P_{out}\left[\left(j+\frac{1}{2}\right)a_i\Delta p\right] - P_{out}\left[\left(j-\frac{1}{2}\right)a_i\Delta p\right], \quad (6)$$
$$j = 1, \ldots, N-1.$$

Equation (5) is a system of nonlinear algebraic equations, whose unknown parameters are the N slice durations Δt_j, as well as the power interval Δp. A necessary condition for this system to be solved is that the number of equations M (thus, the number of average output power measurements) be $\geq N+1$. Again, $M > N+1$ can help to avoid multiple solutions.

In the power range where the slope of the output power characteristic is negative, the values of ΔP_j are negative, so that the corresponding terms in the left-hand side of Eq. (5) are also negative. Graphically, the areas of the corresponding rectangles are subtracted from the underlying rectangles (dashed lines in Fig. 6). Hence, the troughs in the output pulse profile are properly reproduced using this procedure. Solving the system in Eq. (5) yields the width Δt_j and height Δp of each pulse slice, but no information is provided about the temporal position of the rectangles in the pulse profile, so that some type of symmetry has to be assumed. Also, the possibility of a trough in the input pulse profile was discarded, as this would require splitting some slices into multiple segments, whose temporal position could not be restored. Like the case of vertical slicing, it is, thus, assumed that the profile decays monotonically from its peak, either symmetrically on both sides (slices are centered) or asymmetrically on one side (slices aligned on one edge). Finally, to avoid unphysical results, we imposed $\Delta t_j \geq \Delta t_{j+1}$ for $j = 0, \ldots, N-2$.

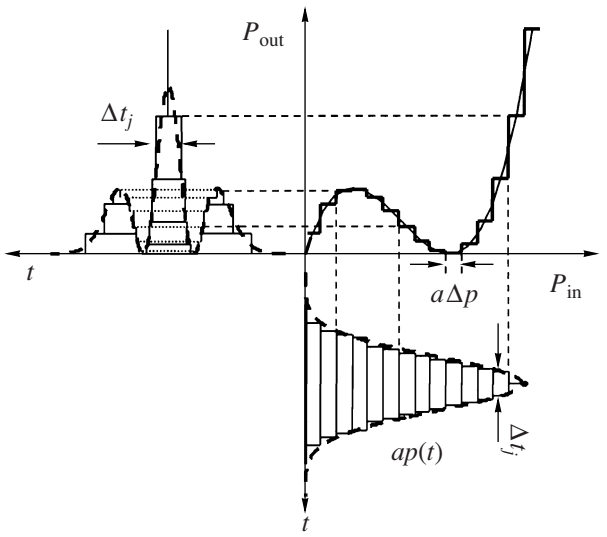

Fig. 6. Principle of horizontal slicing operation in the general case.

We numerically resolved system of equations (5) by the least-squares method, using the same input pulse profiles as those used for vertical slicing (Fig. 7). Again, we used Eq. (1) with $\Delta\phi = \pi/5$. In this case, initial estimations for both Δt_j and Δp were required. A symmetric profile was assumed. A Gaussian was chosen as the initial profile estimation in all cases (this choice was not critical). We used $N \approx 20$ points across the half profile, and $M - N \approx 1$–5. The E_{out} values were calculated through numerical integration of $P_{out}[a_i p(t)]$. Peak powers ranged from $a_i = 0$ to ~$0.3P_\pi$, thus using T well below the critical power. Convergence is ensured for initial estimations of the peak power and pulse duration in the range of ~10 dB about the actual values. The figure shows that sharp edges are, in this case, outlined by a large number of points (Figs. 7d–7f), but only a few points materialize flat tops [Figs. 7d and 7e] or pedestals (Fig. 7f). In addition, in some cases, a fictitious high-power peak of a short duration is added to the pulse profile (Figs. 7d and 7e). Finally, for $\Delta\phi = 0$ and <0, the same conclusions as those for vertical slicing are reached.

4. ROBUSTNESS

We numerically studied how inaccuracies in the parameters P_π, K or $\Delta\phi$ in Eq. (1) affect the retrieved pulse profile. For this purpose, one of these parameters was multiplied by an error factor ε for the calculation of

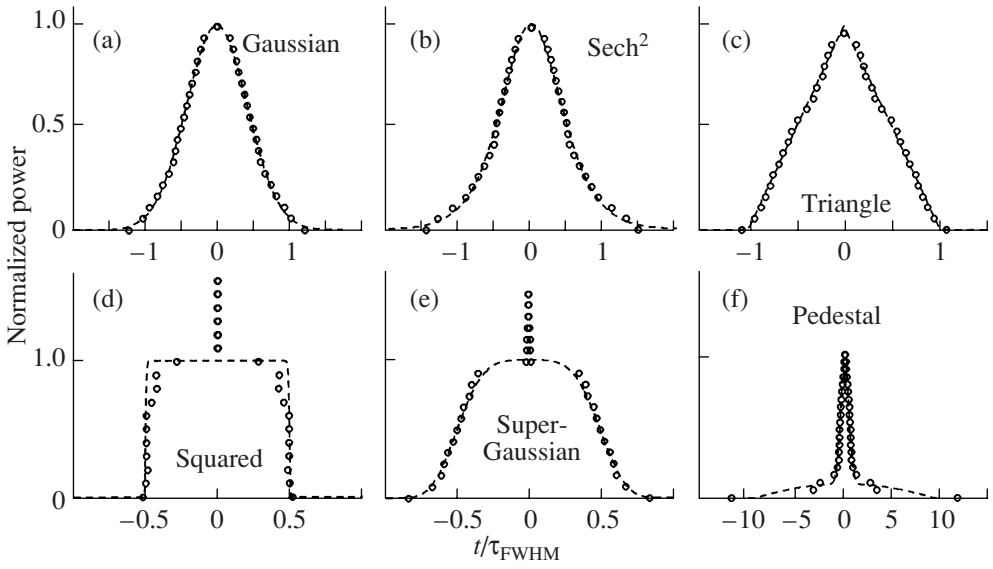

Fig. 7. Results of the horizontal slicing technique for the same profiles and with the same legend as in Fig. 4.

the values of P_{out} and ΔP_j used in the left-hand sides of Eqs. (4) and (5). In contrast, the values of E_{out} in the right-hand sides were simulated using the actual values of these parameters (in a real situation, this amounts to assuming that the E_{out} measurements were correct). First, let us consider an error on K. Figure 8a shows that, in this case, the duration of the retrieved pulse is altered with respect to the actual duration by a factor $1/\varepsilon$ so as to maintain the values of the pulse energy. It should be noted, however, that, as the shape and input power scaling of the T characteristic is not altered, the correct pulse shape and peak power are still obtained. Finally, let us mention that the same distortion is obtained if, instead of an error on K, an error by a factor of $1/\varepsilon$ affects the values of E_{out} (an error in the calibration of the energy scale).

We also simulated the effect of an error ε on the switching power P_π. This corresponds to an error in the calibration of the input power scale. As a result, the peak power of the retrieved profile is altered by the same factor ε. Moreover, to keep the pulse energy values unchanged, the pulse duration is altered by factor $1/\varepsilon$. In contrast, the pulse shape is not altered by this error (Fig. 8b).

Finally, we simulated the effect of an error ε on the phase shift $\Delta\phi$. As this error affects the position of the transmission minimum p_z, the effects on the pulse peak power and duration are analogous to an error on P_π, although the alterations appear to be stronger in this case for the same value of ε (Fig. 8c). In addition, and contrary to the former cases, an error on $\Delta\phi$ also substantially alters the retrieved pulse shape. In practice, errors on parameters P_π, K, or $\Delta\phi$ (and on E_{out}) are likely to appear together, thus distorting the retrieved pulse peak power, duration, and shape. Hence, care must be taken to characterize the NOLM transmission characteristic as precisely as possible in order to ensure a reliable pulse profile measurement. Particular effort should be made towards an accurate determination of $\Delta\phi$, since inaccuracy in this parameter yields severe pulse profile distortions.

In practice, pulses are usually accompanied by noise, in particular amplitude noise, so that its effect on the pulse profile characterization was also analyzed numerically. Considering that the energy at the NOLM output is measured after averaging over many pulses in a train, amplitude noise will alter the E_{out} characteristic, which in turn will modify the retrieved pulse profile. Simulations show, however, that the procedure presents some tolerance to noise. The profiles are not severely distorted for a relative (Gaussian) noise magnitude up to ~15% if $\Delta\phi > 0$, but only up to ~5% if $\Delta\phi < 0$ (Fig. 8d). This demonstrates the poor robustness to noise for a negative $\Delta\phi$, which must be related to the limited profile dependence of the E_{out} characteristic observed in this case, as mentioned previously. For this reason, a positive $\Delta\phi$ should be preferred in practice. If the amplitude noise is excessive, however, its effect can be avoided by performing single-shot energy measurements (detecting simultaneously one input pulse and the corresponding output pulse).

Let us mention finally that, although all results presented in Fig. 8 were obtained using the vertical slicing technique, horizontal slicing was also studied in terms of its robustness, and results very similar to those discussed here were obtained in this case.

5. EXPERIMENTAL RESULTS

We tested both the vertical and horizontal slicing techniques experimentally. We used a NOLM operating

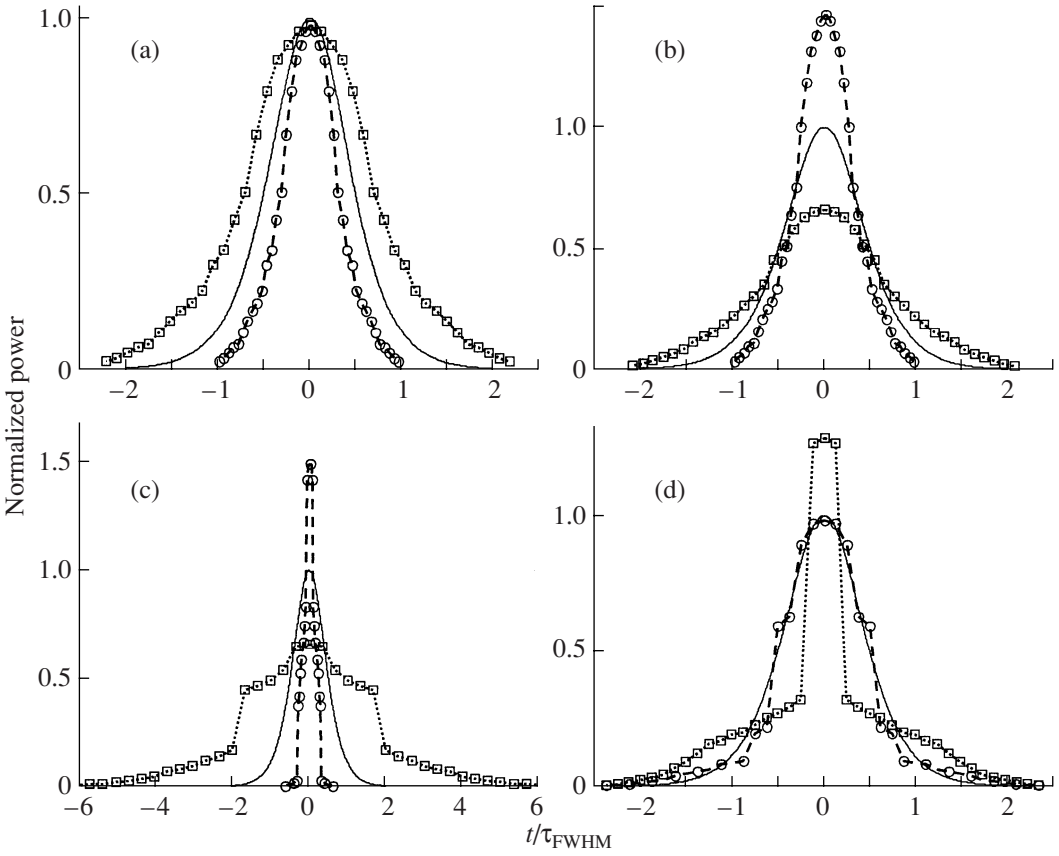

Fig. 8. Distortions of the retrieved pulse profile (here, a squared secant hyperbolic) when either (a) K, (b) P_π, or (c) $\Delta\phi$ is overestimated (circles) and underestimated (squares) by a factor of 1.5; actual phase shift $\Delta\phi = \pi/5$; (d) effect of Gaussian amplitude noise with a 15% standard deviation for $\Delta\phi = \pi/5$ (circles) and $\Delta\phi = -\pi/5$ (squares). Solid lines correspond to target. The vertical slicing technique was used in all cases; τ_{FWHM} is full width at half maximum pulse duration.

through a nonlinear polarization rotation (NPR) [20], including a 50/50 coupler, 500 m of a highly twisted (7 turns/m) standard SMF-28 fiber, and a quarter-wave plate (QWP, Fig. 9). Twisting the fiber allows us to eliminate the residual birefringence, preventing NPR from averaging out [21]. Twisting also makes the device environmentally stable, avoiding drifts of the T characteristic, a key condition for the proper pulse profile characterization. The input signal to the NOLM was circularly polarized. Transmission through polarizer P1 was maximized using a polarization controller. Selecting the orthogonal circular component at the NOLM output yields the T characteristic given by Eq. (1), with $P_\pi \approx 30$ W, where $\Delta\phi$ can be adjusted simply by the QWP angle α [22]. The input and output pulses were detected with two InGaAs 1-GHz detectors.

The angle α was adjusted to have a minimum T at a small value of P_{in}. Transmission was measured using ns-squared optical pulses from a directly modulated DFB laser diode emitting at 1549 nm. The laser was biased below the threshold and modulated by *ns*-squared current pulses at a rate of 100 Hz. The optical pulses were amplified by a two-stage erbium-doped fiber amplifier (EDFA) and launched into the NOLM. The detected input and output pulses were monitored on a two-channel 500-MHz oscilloscope (in the average mode), allowing us to resolve the pulse profiles. Transmission was measured between 0 and ~11 W (thus, well below P_π) by adjusting the amplitude of the current pulses. The inset in Fig. 10a shows the measured T between 0 and 6 W. It includes the insertion loss of the output polarizer. Fitting the experimental data using Eq. (1) led to $\Delta\phi = \pi/10$ with a minimal $T > 0$, which does not hinder the proper profile determination.

In the first experiment, we used 30-ns-squared pulses, produced as described above (using 30-ns current pulses). Although the practical interest for the techniques may be limited for such wide pulses, this experiment offers the possibility of precisely assessing the performances of the techniques by comparison with the actual profile, which can be easily obtained using a conventional scope measurement. The waveform was measured on a 500-MHz scope (Figs. 10b and 10c, solid), including a roughly constant plateau and a 2-ns initial pulse (this duration was confirmed by a 10-GHz sampling scope measurement). For various values of the

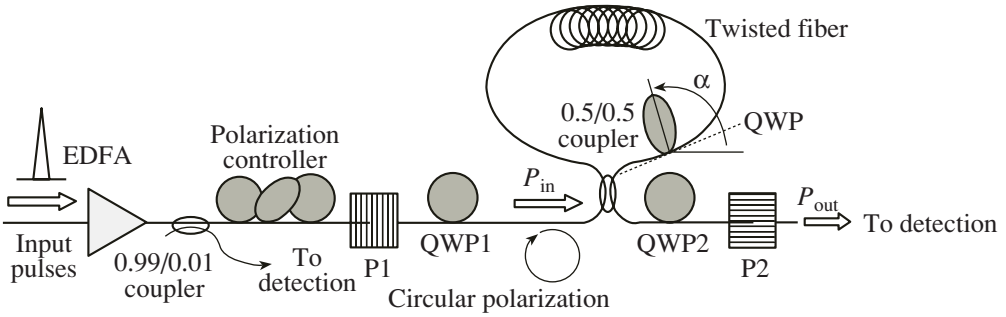

Fig. 9. Experimental setup. P1 and P2 are linear polarizers.

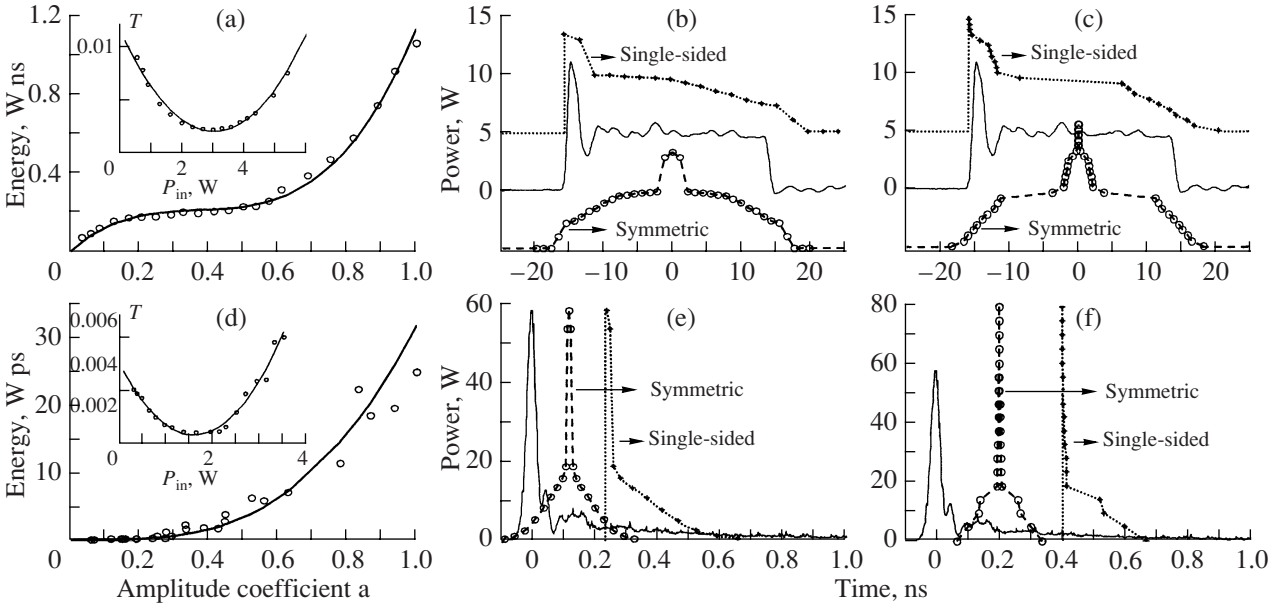

Fig. 10. (a, d) E_{out} characteristic recalculated from the retrieved profile and NOLM transmission (insets): dots experiment and (lines) fit (inset); (b, e) pulse profiles recovered using vertical slicing and (c, f) using horizontal slicing, for pulses from the DFB laser (a–c) and from the F8L (d, e, f). Curves in (b–f) were shifted for better readability.

input power (plateau power between 0–4 W), E_{out} was measured through the impulse response resulting from the output waveform detection on a low-bandwidth (20-MHz) oscilloscope (Fig. 10a, circles). In the optimization procedures, a Gaussian profile was used as the initial estimate. We used $N = 20$ and $M - N = 2$. The retrieved profiles (single-sided and symmetric) are shown in Fig. 10b for vertical slicing and in Fig. 10c for horizontal slicing. The E_{out} characteristic recalculated using the profile retrieved by vertical slicing is shown in Fig. 10a (solid). A similar curve was obtained from the results of horizontal slicing (not shown). A waveform with a ~3-ns pulse and a ~30-ns plateau is obtained in each case, with power values close to the expected values. In the case of vertical slicing, numerous points define the plateau, but only a few points outline the peak, whereas the contrary occurs for horizontal slicing. In the latter case, a fictitious thin peak is added at the top of the profile, making it difficult to estimate the peak power. This does not occur for vertical slicing. Hence, it appears that both vertical and horizontal slicing techniques are complementary. However, they are equally unable to determine the position of the 2-ns pulse in the waveform. Also, the deep trough observed just after the pulse in the actual waveform cannot be restituted, although it affects the recovered waveforms through the smooth decay of the plateau at the waveform edges (see Figs. 10b and 10c).

In the second experiment, we considered *ps* pulses from a figure-eight fiber laser (F8L). Figures 10e and 10f (solid) shows the pulse measured with a fast photodetector (10-GHz specified bandwidth) and a 20-GHz

sampling scope in the average mode. The curve shows a ~30-ps pulse followed by a ~1-ns tail. This measurement allows for the determination of the tail extension, but not the pulse duration due to the bandwidth limitations of the setup. Accurate measurement of the pulse duration was performed through optical autocorrelation, yielding a full width at half maximum duration $\tau_{FWHM} \approx 22$ ps (assuming a Gaussian pulse). The autocorrelation presented substantial background related to the waveform tail. However, its duration could not be estimated with the autocorrelator due to its limited scanning range. The precise assessment of the waveform thus required both scope and autocorrelation measurements.

The NOLM transmission was again measured using squared *ns* pulses for powers between 0 and ~15 W (Fig. 10d, inset shows T between 0 and 4 W). Fitting using Eq. (1) yielded $\Delta\phi = 0.054\pi$. Pulses from the F8L were launched into the NOLM. Due to a large amplitude noise affecting the pulses, the input and output were monitored simultaneously using a two-channel 500-MHz oscilloscope in the single-shot mode (triggered off the input pulse). The amplitude noise was high enough to select the input pulse power over a wide range, simply by adjusting the trigger level (in the case of stable pulses, an adjustable attenuator must be used at the NOLM input). For each value of the input power, the measurement of the impulse response of the output waveform on the 500-MHz scope yielded E_{out} (Fig. 10d, circles). Again, for both vertical and horizontal slicing, a Gaussian profile was used as the initial estimate. We used $N = 25$ and $M - N = 5$ in both cases. The profiles retrieved under symmetric or single-sided assumptions are shown in Fig. 10e for vertical slicing and in Fig. 10f for horizontal slicing. The E_{out} characteristic recalculated using the profile retrieved by vertical slicing is shown in Fig. 10d (solid). A similar curve was obtained from the results of horizontal slicing (not shown). For both techniques, the recovered waveform includes a ~15–20-ps pulse and a wide pedestal about half as long and twice as high as the actual tail. The waveforms are quite close to the expected profile given the precision of the measurements. Again, the techniques are unable to determine the position of the pulse in the waveform. As previously stated, vertical slicing yields a better resolution of the pedestal, whereas the pulse is better outlined by horizontal slicing. This shows, once more, that both techniques complement each other for proper profile retrieval. Again, horizontal slicing adds a fictitious thin peak to the waveform, so that the peak power is better assessed through vertical slicing. Figure 10e shows that the highest peak power reached in the experiment is ~60 W at the F8L output (~13 W into the NOLM). In contrast, the pulse peak power could not be measured with precision using the sampling scope due to the large noise.

6. CONCLUSIONS

In conclusion, we proposed in this work a technique to characterize the temporal power profile of short pulses, which exploits the nonlinear transfer characteristic of a fiber NOLM. The technique is based on the observation that, for a particular NOLM power transfer function with a nonzero phase bias, the output energy versus input energy characteristic of the pulses is specific to each profile. Measuring this energy transfer characteristic at a moderate power then allows the retrieval of the unknown profile. This measurement can be done with a low-frequency detection setup, making the technique affordable. Two numerical approaches are considered, both relying on the resolution of a system of nonlinear algebraic equations. In the first approach, the profile is vertically split into a finite series of rectangles of unknown power (vertical slicing), and in the second, it is divided horizontally into a finite stack of rectangles of unknown duration (horizontal slicing). We showed numerically and experimentally that both approaches allow for the proper profile retrieval for a wide variety of pulse shapes. Flat regions in the waveform (plateau, pedestal) are better outlined and the peak power is better estimated through vertical slicing, whereas horizontal slicing better outlines sharp edges and short features, so that the two approaches are complementary. We also showed through numerical simulations that precise knowledge of the NOLM transmission characteristic is essential in order to avoid distortions of the retrieved profile. In contrast, the technique presents some tolerance to amplitude noise. As long as the peak power remains well below the critical power, parasitic nonlinear effects such as Raman or Brillouin scattering can be avoided. The technique is applicable to a wide range of pulse durations, from a few *ps* to a few *ns*, without modification of the setup. The profiles of monotonous and symmetric pulses are retrieved without ambiguity. Although the temporal sequence of features in complex waveforms cannot be restored, valuable information such as the duration, peak power, and temporal distribution of instantaneous power across the pulse is retrieved. We believe that this technique could advantageously complement conventional techniques for characterizing the temporal profile of short and even ultrashort pulses down to a few *ps* in duration.

ACKNOWLEDGMENTS

O. Pottiez was supported by CONCYTEG grant no. 07-04-K662-043 and by CONACyT grant no. 53990.

REFERENCES

1. J.-C. Diels and W. Rudolph, *Ultrashort Laser Pulse Phenomena. Fundamentals, Techniques, and Applications on a Femtosecond Time Scale* (Academic, San Diego, 1996), Chap. 8.

2. D. Meshulach, Y. Barad, Y. Silberberg, J. Opt. Soc. Am. B **14**, 2122 (1997).
3. D.J. Kane, R. Trebino, IEEE J. Quantum Electron. **29**, 571 (1993).
4. J. W. Nicholson, J. Jasapara, W. Rudolph, et al., Opt. Lett. **24**, 1774 (1999).
5. T.-M. Liu, Y.-C. Huang, G.-W. Chern, et al., Appl. Phys. Lett. **81**, 1402 (2002).
6. S. H. Chin, Y. J. Kim, H. S. Song, and D. Y. Kim, Appl. Opt. **45**, 7718 (2006).
7. C. Iaconis and I. A. Walmsley, Opt. Lett. **23**, 792 (1998).
8. K. C. Chu, J. P. Heritage, R. S. Grant, et al., Opt. Lett. **20**, 904 (1995).
9. J. E. Rothenberg and D. Grischkowsky, Opt. Lett. **12**, 99 (1987).
10. I. Kang, C. Dorrer, and F. Quochi, Opt. Lett. **28**, 2264 (2003).
11. N. K. Berger, B. Levit, and B. Fisher, Electron. Lett. **37**, 1033 (2001).
12. N. K. Berger, B. Levit, V. Smulakovsky, and B. Fisher, Appl. Opt. **44**, 7862 (2005).
13. S. Prein, S. Diddams, and J.-C. Diels, Opt. Comm. **123**, 567 (1996).
14. P. Kockaert, J. Azaña, L. R. Chen, and S. LaRochelle, IEEE Photonics Technol. Lett. **16**, 1540 (2004).
15. D. N. Fittinghoff, J. L. Bowie, J. N. Sweetser, et al., Opt. Lett. **21**, 884 (1996).
16. D. Meshulach, D. Yelin, and Y. Silberberg, J. Opt. Soc. Am. B **14**, 2095 (1997).
17. N. J. Doran and D. Wood, Opt. Lett. **13**, 56 (1988).
18. R. Adams, M. Rochette, T. T. Ng, and B. J. Eggleton, IEEE Photonics Technol. Lett. **18**, 469 (2006).
19. O. Pottiez, B. Ibarra-Escamilla, and E. A. Kuzin, IEEE Photonics Technol. Lett. **19**, 1347 (2007).
20. E. A. Kuzin, N. Korneev, J. W. Haus, and B. Ibarra-Escamilla, J. Opt. Soc. Am. B **18**, 919 (2001).
21. T. Tanemura and K. Kikuchi, J. Lightwave Technol. **24**, 4108 (2006).
22. O. Pottiez, E. A. Kuzin, B. Ibarra-Escamilla, and F. Mendez Martinez, Opt. Comm. **229**, 147 (2004).